PERGAMON

Scripta mater. 42 (2000) 781–787

Scripta MATERIALIA

www.elsevier.com/locate/scriptamat

ANALYTICAL MODELING OF OXIDE THICKNESS EFFECTS ON RESIDUAL STRESSES IN THERMAL BARRIER COATINGS

C.H. Hsueh[1] and E.R. Fuller, Jr.[2]

[1] Oak Ridge National Laboratory, Oak Ridge, Tennessee 37831-6068

[2] National Institute of Standards and Technology, Gaithersburg, Maryland 20899

(Received September 27, 1999)
(Accepted in revised form December 2, 1999)

Keywords: Modeling; Thermal barrier coating; Thermal expansion; Stress

Introduction

During high temperature operation, an oxide scale forms along the irregular top coat/bond coat interface in the plasma-sprayed thermal barrier coating (TBC) system. The residual stresses in the system are affected by the presence of the thermally grown oxide (TGO) [1–5]. Along the irregular interface, the asperity can be convex or concave. Semicircular convex and concave asperities have been adopted for numerical simulations to examine the effects of the TGO thickness on residual thermal stresses [6]. It was found that in the tip region of a convex asperity, the residual stress normal to the interface, σ_y, in the ceramic top coat is tensile for a thin oxide but becomes compressive for a thick oxide. In the tip region of a concave asperity, σ_y in the ceramic top coat is compressive for a thin oxide and becomes less compressive for a thick oxide.

The purpose of the present study was to explore the physical meaning of the trend of the stress state of σ_y in the ceramic top coat with the variation of the TGO thickness. To achieve this, a simple analytical model of three concentric circles was adopted. First, the residual thermal stresses in the three-concentric-circles model were derived. Then, the results for residual radial stresses at the top coat/TGO and the TGO/bond coat interfaces as functions of the TGO thickness were presented. Also, the physical meaning of the above results was discussed.

Analytical Modeling

A two-concentric-circles model has been used previously to study the residual stresses in a coating formed on a wrinkled substrate [7,8]. A three-concentric-circles model is hence adopted in the present study to simulate the wrinkle geometry in a TBC system. A circular region of phase 1 with a radius a is surrounded by a concentric annulus of phase 2 with an outer radius b which is then surrounded by another concentric annulus of phase 3 with an outer radius c (see Fig. 1). Whereas phases 1, 2, and 3 are designated respectively as the bond coat, the TGO, and the top coat in modeling a convex asperity, they are designated respectively as the top coat, the TGO, and the bond coat in modeling a concave asperity. In both cases, the TGO thickness is dictated by b-a.

Residual thermal stresses develop during the temperature change in the system because of the thermal-mechanical mismatch among the three phases. The stresses can be determined by the procedure

1359-6462/00/$–see front matter. © 2000 Acta Metallurgica Inc. Published by Elsevier Science Ltd. All rights reserved.
PII: S1359-6462(99)00430-3

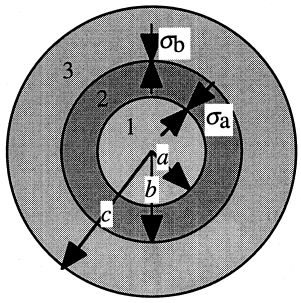

Figure 1. A schematic showing the three-concentric-circles model.

of first allowing the three phases to exhibit unconstrained differential thermal strains during the temperature change. Then, radial stresses, σ_a and σ_b, are placed at the interfaces, $r = a$ and $r = b$, respectively to restore the displacement continuity at the two interfaces. With interfacial radial stresses, σ_a and σ_b, the radial and the tangential stresses in phases 1, 2, and 3 are

$$\sigma_{1,r} = \sigma_a \tag{1a}$$

$$\sigma_{1,t} = \sigma_a \tag{1b}$$

$$\sigma_{2,r} = \frac{a^2b^2(\sigma_a - \sigma_b)}{r^2(b^2 - a^2)} - \frac{a^2\sigma_a - b^2\sigma_b}{b^2 - a^2} \tag{2a}$$

$$\sigma_{2,t} = \frac{-a^2b^2(\sigma_a - \sigma_b)}{r^2(b^2 - a^2)} - \frac{a^2\sigma_a - b^2\sigma_b}{b^2 - a^2} \tag{2b}$$

$$\sigma_{3,r} = \frac{b^2(c^2 - r^2)\sigma_b}{r^2(c^2 - b^2)} \tag{3a}$$

$$\sigma_{3,t} = \frac{-b^2(c^2 + r^2)\sigma_b}{r^2(c^2 - b^2)} \tag{3b}$$

where r is the distance from the center of the circles, the subscripts 1, 2, and 3 denote phases 1, 2, and 3, and the subscripts r and t denote the radial and the tangential components, respectively.

With a temperature change, ΔT, the strain consists of two components: the elastic strain and the unconstrained thermal strain. The tangential strains in phases 1, 2, and 3, $\epsilon_{1,t}$, $\epsilon_{2,t}$, and $\epsilon_{3,t}$, are respectively

$$\epsilon_{1,t} = \frac{\sigma_{1,t} - \nu_1\sigma_{1,r}}{E_1} + \alpha_1\Delta T \tag{4}$$

$$\epsilon_{2,t} = \frac{\sigma_{2,t} - \nu_2\sigma_{2,r}}{E_2} + \alpha_2\Delta T \tag{5}$$

$$\epsilon_{3,t} = \frac{\sigma_{3,t} - \nu_3\sigma_{3,r}}{E_3} + \alpha_3\Delta T \tag{6}$$

where E, ν, and α are Young's modulus, Poisson's ratio, and the coefficient of thermal expansion (CTE), respectively.

The residual stresses in the system are contingent upon the solutions of the interfacial radial stresses, σ_a and σ_b, which can be determined by the continuity condition at the interface. Continuity of the radial displacement at the interface is required. With the tangential strain proportional to the radial displacement, this continuity condition becomes

$$\epsilon_{1,t} = \epsilon_{2,t} \qquad (\text{at } r = a) \tag{7}$$

$$\epsilon_{2,t} = \epsilon_{3,t} \qquad (\text{at } r = b) \tag{8}$$

Combination of Equations (1) through (8), yields

$$\sigma_a = \frac{E_2[P_1(\alpha_2 - \alpha_1) + P_4(\alpha_3 - \alpha_2)]\Delta T}{P_1P_2 - P_3P_4} \tag{9}$$

$$\sigma_b = \frac{E_2[P_3(\alpha_2 - \alpha_1) + P_2(\alpha_3 - \alpha_2)]\Delta T}{P_1P_2 - P_3P_4} \tag{10}$$

where the parameters, P_1, P_2, P_3, and P_4, are given by

$$P_1 = \frac{b^2 + a^2}{b^2 - a^a} - \nu_2 + \frac{E_2}{E_3}\left(\frac{c^2 + b^2}{c^2 - b^2} + \nu_3\right) \tag{11a}$$

$$P_2 = \frac{b^2 + a^2}{b^2 - a^a} + \nu_2 + \frac{E_2(1 - \nu_1)}{E_1} \tag{11b}$$

$$P_3 = \frac{2a^2}{b^2 - a^2} \tag{11c}$$

$$P_4 = \frac{2b^2}{b^2 - a^2} \tag{11d}$$

The stress state at $r = b$ (i.e., σ_b is tensile or compressive) depends on the comparison between α_3 and the effective CTE in the region of $r<b$ which is a function of dimensions, elastic constants, and CTEs of phases 1 and 2. This effective CTE, α_{12}, is dictated by the radial displacement at $r = b$ in the absence of phase 3, and has been derived previously, such that [9]

$$\alpha_{12} = \alpha_2 + \frac{P_3(\alpha_1 - \alpha_2)}{P_2} \tag{12}$$

In the specific case of $E_1 = E_2$ and $\nu_1 = \nu_2$, Equation (12) becomes

$$\alpha_{12} = \frac{a^2\alpha_1 + (b^2 - a^2)\alpha_2}{b^2} \qquad (\text{for } E_1 - E_2 \text{ and } \nu_1 = \nu_2) \tag{13}$$

Hence, when phases 1 and 2 have the same elastic constants, the effective CTE, α_{12}, can be obtained using rule-of-mixtures.

Similarly, the stress state at $r = a$ depends on the comparison between α_1 and the effective CTE in the region of $a<r<c$ which is a function of dimensions, elastic constants, and CTEs of phases 2 and 3. This effective CTE, α_{23}, is dictated by the radial displacement at $r = a$ in the absence of phase 1. Using the similar technique as that for deriving α_{12}, α_{23} can be obtained, such that

$$\alpha_{23} = \alpha_2 + \frac{P_4(\alpha_3 - \alpha_2)}{P_1} \qquad (\text{at } r = a) \tag{14}$$

In the specific case of $E_2 = E_3$ and $\nu_2 = \nu_3$, Equation (14) becomes

$$\alpha_{23} - \frac{(b^2 - a^2)\alpha_2 + (c^2 - b^2)\alpha_3}{c^2 - a^2} \qquad (\text{for } E_2 = E_3 \text{ and } \nu_2 = \nu_3) \tag{15}$$

Hence, when phases 2 and 3 have the same elastic constants, the effective CTE, α_{23}, can also be obtained using rule-of-mixtures. It can also be derived that when the radial displacement at $r = c$ is considered, the effective CTE, α_{23}, becomes

$$\alpha_{23} = \alpha_3 - \frac{2b^2E_2(\alpha_3 - \alpha_2)}{(c^2 - b^2)P_1E_3} \qquad (\text{at } r = c) \tag{16}$$

It is noted that Equation (16) is different from Equation (14). Nevertheless, when phases 2 and 3 have the same elastic constants, Equation (16) also becomes Equation (15). However, to determine the stress state at $r = a$, comparison should be made between α_1 and α_{23} given by Equation (14).

Using the definitions of α_{12} and α_{23} in Equations (12) and (14), α_a and α_b in Equations (9) and (10) become

$$\sigma_a = \frac{P_1E_2(\alpha_{23} - \alpha_1)\Delta T}{P_1P_2 - P_3P_4} \tag{17}$$

$$\sigma_b = \frac{P_2E_2(\alpha_3 - \alpha_{12})\Delta T}{P_1P_2 - P_3P_4} \tag{18}$$

When a three dimensional geometry is considered, a three-concentric-spheres model can be used. The analytical steps for deriving the residual thermal stresses in the three-concentric-spheres model are similar to those for the three-concentric-circles model. The solutions for α_{12}, α_{23}, α_a, and α_b have the same general forms as those for the three-concentric-circles model [i.e., Equations (12), (14), (17), and (18)]. However, the parameters, P_1, P_2, P_3, and P_4, become

$$P_1 = \frac{2b^3(1 - 2\nu_2) + a^3(1 + \nu_2)}{2(b^3 - a^3)} + \frac{E_2}{E_3}\left[\frac{c^3(1 + \nu_3) + 2b^3(1 - 2\nu_3)}{2(c^3 - b^3)}\right] \tag{19a}$$

$$P_2 = \frac{b^3(1 + \nu_2) + 2a^3(1 - 2\nu_2)}{2(b^3 - a^3)} + \frac{E_2(1 - 2\nu_1)}{E_1} \tag{19b}$$

$$P_3 = \frac{3a^3(1 - \nu_2)}{2(b^3 - a^3)} \tag{19c}$$

$$P_4 = \frac{3b^3(1 - \nu_2)}{2(b^3 - a^3)} \tag{19d}$$

Results

The residual stresses calculated from the three-concentric-circles model were presented in the present study. The thermal/mechanical properties pertinent to the air plasma-sprayed TBC system of ZrO_2 top coat/α-Al_2O_3 TGO/vacuum plasma-sprayed Ni-22Cr-10Al-1Y bond coat listed in Table 1 were adopted

TABLE 1
The Thermal/Mechanical Properties of the Plasma Sprayed TBC System

	Young's Modulus, E (GPa)	Poisson's Ratio, ν	CTE ($\times 10^{-6}$/°C)
Top Coat	50	0.1	10
Oxide Scale	360	0.27	8
Bond Coat	200	0.3	15.2

for calculations. The temperature change, ΔT, used in calculating the thermal strain was -1125°C. Young's modulus, E, was replaced by $E/(1-\nu)$ before it was substituted into the analytical solutions due to the biaxial stress state in the TBC system as discussed in Refs. [2–5].

For a convex asperity, phases 1, 2, and 3 correspond to the bond coat, the TGO, and the top coat, respectively. The residual radial stresses at $r = a$ and $r = b$ (i.e., σ_a and σ_b) as functions of the normalized TGO thickness, $(b-a)/a$, are shown in Fig. 2a for $c/a = 5$, 10, and 20. In this case, σ_b corresponds to σ_y in the top coat at the tip of a convex asperity. The stresses are not sensitive to c/a when $c/a \geq 5$. The results for $c/a = 10$ almost overlap with those for $c/a = 20$, and cannot be distinguished in Fig. 2a. While σ_a is tensile and increases with the TGO thickness, σ_b is tensile when $(b-a)/a < \sim 0.75$ and becomes compressive when $(b-a)/a > \sim 0.75$. The effective CTE, α_{12}, as a function of the normalized TGO thickness, $(b-a)/a$, is shown in Fig. 2b. It is noted that α_{12} is independent of c [see Equation (12)]. The CTE of phase 3, α_3 ($=10\times10^{-6}$/°C), is also shown in Fig. 2b. It can be seen that $\alpha_{12} > \alpha_3$ when $(b-a)/a < \sim 0.75$ which, in turn, results in a tensile residual radial stress at $r = b$ during cooling. Conversely, $\alpha_{12} < \alpha_3$ when $(b-a)/a > \sim 0.75$ which, in turn, results in a compressive residual radial stress at $r = b$ during cooling.

For a concave asperity, phases 1, 2, and 3 correspond to the top coat, the TGO, and the bond coat, respectively. The residual radial stresses at $r = a$ and $r = b$ as functions of the normalized TGO thickness, $(b-a)/a$, are shown in Fig. 3a at different c/a ratios. In this case, σ_a corresponds to σ_y in the top coat at the tip of a concave asperity. The stresses are not sensitive to c/a when $c/a \geq 10$. While σ_b is compressive and its magnitude increases with the TGO thickness for $c/a \geq 10$, σ_a becomes less compressive with the increasing TGO thickness and decreasing c/a for the dimension considered in Fig. 3a. The effective CTE, α_{23}, as a function of the normalized TGO thickness, $(b-a)/a$, is shown in Fig. 3b at different c/a ratios. The CTE of phase 1, α_1 ($=10\times10^{-6}$/°C), is also shown. It can be seen that

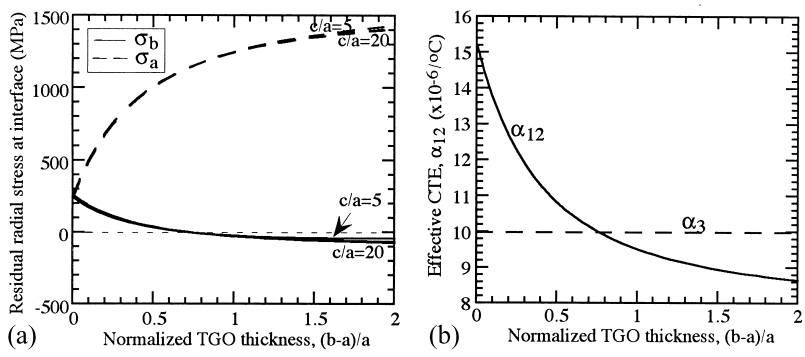

Figure 2. (a) The residual radial stress at the TGO/bond coat interface, σ_a, and at the top coat/TGO interface, σ_b, and (b) the effective CTE, α_{12}, for the region $r<b$, and the CTE of top coat, α_3, as functions of the normalized TGO thickness, $(b-a)/a$, at different c/a ratios for a convex asperity.

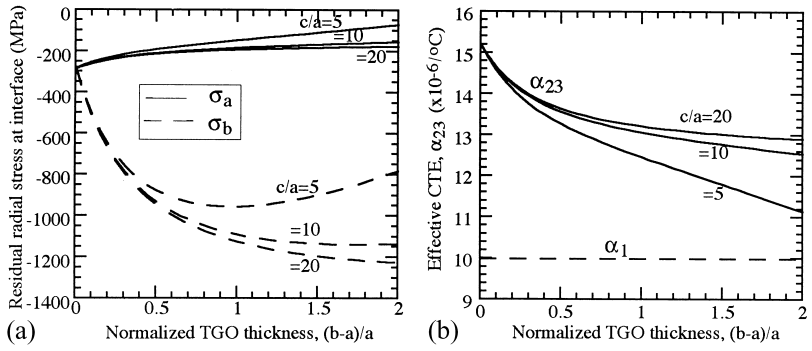

Figure 3. (a) The residual radial stress at the top coat/TGO interface, σ_a, and at the TGO/bond coat interface, σ_b, and (b) the effective CTE, α_{23}, for the region $a<r<c$, and the CTE of top coat, α_1, as functions of the normalized TGO thickness, $(b - a)/a$, at different c/a ratios for a concave asperity.

$\alpha_{23}>\alpha_1$ for the dimension considered in Fig. 3b. However, the difference between α_{23} and α_1 decreases with the increasing TGO thickness and decreasing c/a. Compared to Fig. 2b, Fig. 3b shows that the decrease in α_{23} is much slower than the decrease in α_{12} when the TGO thickness increases. This is due to the fact that the bond coat for a concave asperity (i.e., phase 3 in Fig. 1) has a much greater area than that for a convex asperity (i.e., phase 1 in Fig. 1) in the three-concentric-circles model, and the effect of the TGO thickness on the effective CTE is much weaker for a concave asperity than for a convex asperity.

Conclusions

The residual thermal stress normal to the interface in the ceramic top coat and close to the TGO is of interest, since it could result in cracking and spallation of the plasma-sprayed TBC. The effects of the TGO thickness on this residual stress were qualitatively interpreted in the present study by using an analytical model of three concentric circles (Fig. 1). An effective CTE was defined to illustrate the qualitative trends of the TGO thickness effects. To model a convex interface asperity, phases 1, 2, and 3 in Fig. 1 correspond to bond coat, TGO, and top coat, respectively. The residual radial stress at $r = b$ (i.e., at the top coat/TGO interface), σ_b, is of interest. The stress state of σ_b can be obtained by comparing α_3 with the effective CTE in the region of $r<b$ which is a function of dimensions, elastic constants, and CTEs of phases 1 and 2 (Fig. 2). To model a concave interface asperity, phases 1, 2, and 3 in Fig. 1 correspond to top coat, TGO, and bond coat, respectively. The residual radial stress at $r = a$ (i.e., at the top coat/TGO interface), σ_a, is of interest. The stress state of σ_a can be obtained by comparing α_1 with the effective CTE in the region of $a<r<c$ which is a function of dimensions, elastic constants, and CTEs of phases 2 and 3 (Fig. 3).

Acknowledgments

CHH acknowledges jointly support of the U.S. Department of Energy, Division of Materials Sciences, Office of Basic Energy Sciences, and Assistant Secretary for Energy, Efficiency and Renewable Energy, Office of Industrial Technologies, Advanced Turbine Systems Program, under contract DE-AC05-96OR22464 with Lockheed Martin Energy Research Corp. ERF acknowledges support of the Alexander von Humboldt Foundation.

References

1. J. A. Haynes, E. D. Rigney, M. K. Ferber, and W. D. Porter, Surf. Coat. Technol. 86–87, 102 (1996).
2. R. J. Christensen, V. K. Tolpygo, and D. R. Clarke, Acta Mater. 45, 1761 (1997).
3. A. G. Evans, M. Y. He, and J. W. Hutchinson, Acta Mater, 45, 3543 (1997).
4. A. M. Freborg, B. L. Ferguson, W. J. Brindley, and G. J. Petrus, Mater. Sci. Eng. A245, 182 (1998).
5. C. H. Hsueh, J. A. Haynes, M. J. Lance, P. F. Becher, M. K. Ferber, E. R. Fuller, S. A. Langer, W. C. Carter, and W. R. Cannon, J. Am. Ceram. Soc. 82, 1073 (1999).
6. C. H. Hsueh, and E. R. Fuller, unpublished work.
7. C. H. Hsueh, and A. G. Evans, J. Appl. Phys. 54, 6672 (1983).
8. X. Y. Gong, and D. R. Clarke, Oxidation Metals. 50, 355 (1998).
9. C. H. Hsueh, P. F. Becher, and E. Y. Sun, J. Mater. Sci. submitted.